

Analysis of interdomain dynamics in a two-domain protein using residual dipolar couplings together with ^{15}N relaxation data

Yaroslav Ryabov and David Fushman*

Department of Chemistry and Biochemistry, Center for Biomolecular Structure and Organization, University of Maryland, College Park, MD 20742, USA

Received 30 November 2005; Revised 17 February 2006; Accepted 28 February 2006

In this paper, we propose the idea that simultaneous analysis of NMR relaxation data and residual dipolar couplings (RDCs) can provide information about interdomain dynamics in a multidomain protein, which cannot be derived from each data set separately. Specifically, such an approach can be useful when the interdomain motions occur on a timescale comparable to or slower than the overall tumbling in solution. We analyze residual dipolar couplings together with ^{15}N relaxation data for Lys48-linked di-ubiquitin (Ub_2), in which interdomain dynamics are described as interconversion between two distinct conformational states of the protein. Our results show that ^{15}N relaxation and residual dipolar coupling data can be used as two complementary experimental data sets for consistent characterization of interdomain conformations and dynamics in this dual-domain protein. Copyright © 2006 John Wiley & Sons, Ltd.

KEYWORDS: domain dynamics; domain orientation; spin relaxation; residual dipolar couplings; di-ubiquitin; conformational interconversion

INTRODUCTION

Domain motions often play a key role in molecular recognition events and functional regulation in a variety of processes involving multidomain proteins (see examples in Refs 1–3). However, despite recent developments in structure characterization of multidomain systems and changes in interdomain orientation upon ligand binding in solution,^{4–9} very little is known about the actual mechanisms of interdomain dynamics in proteins. The first attempts to use nuclear magnetic resonance (NMR) for characterization of interdomain dynamics in a two-domain protein calmodulin were undertaken by Tjandra *et al.*^{10–12} In that study, ^{15}N relaxation data were treated within the so-called ‘extended model-free’ approach originally developed for intradomain dynamics comprising both fast and slow (yet faster than the overall tumbling) motions.¹³

The idea of cone representation of the conformational space sampled by domain orientations was recently used for the analysis of residual dipolar couplings (RDCs) and pseudocontact shifts measured in calmodulin.¹⁴ In our previous study¹⁵ we suggested a different way of describing interdomain dynamics in a protein. In particular, in the case of Lys48-linked di-ubiquitin (Ub_2) we introduced a model that considered interdomain dynamics as interconversion between two distinct states (ITS) of the protein. The ITS model was found to be more suitable than the

extended model-free paradigm in the case of Ub_2 , which, in contrast to calmodulin, exhibits at least one well-defined conformational state, predominantly populated at neutral and alkaline conditions.¹⁶ Using this model, we were able to fit ^{15}N relaxation data for Ub_2 and adequately describe its dynamics.¹⁵ Moreover, the ITS model provided detailed structural information about domain orientations in each of the interconverting states and the corresponding occupation probabilities, which is impossible to derive from the extended model-free treatment.

In our previous study¹⁵ (also Ryabov and Fushman, in preparation) we used ^{15}N relaxation data for characterization of motions in Ub_2 . Besides the problem of choosing the appropriate model for interdomain dynamics (as mentioned above), dealing with NMR relaxation data in solution brings up another important issue – the upper limit on the timescale of motions accessible by these measurements. Orientational averaging of the spin Hamiltonian by the overall tumbling in an isotropic solution sets a timescale cutoff: all intraprotein reorientational processes considerably slower than the correlation time of the overall rotational diffusion cannot be reliably detected by this relaxation technique.

RDCs (first introduced in Refs 17, 18) have become an important source of long-distance, orientational information for protein structure determination. The crucial idea of this method is to break the symmetry of the (otherwise uniform) distribution of the protein’s orientations by introducing weak molecular alignment. This can be achieved by using the anisotropy of magnetic susceptibility (intrinsic or imposed by paramagnetic tagging) of the molecule^{17,18} or by introducing

*Correspondence to: David Fushman, 1115 Biomolecular Sciences Bldg (#296), University of Maryland, College Park, MD 20742-3360, USA. E-mail: fushman@umd.edu

anisotropy in the medium, e.g. by means of inducing liquid crystalline phase¹⁹ or mechanical strain.^{20,21} In this case the dipolar interaction is not completely averaged by the overall tumbling, which thus opens the possibility of measuring the residual part of the dipolar coupling between nuclei in a protein. The RDC contains information about the length and orientation of the internuclear vector of interest, and, in principle, samples their fluctuations during the course of NMR experiment. However, the RDC data are not directly suitable for investigation of protein dynamics. The main reason is that, as a spectroscopic rather than relaxation technique, this method senses time-averaged spin Hamiltonian, an essentially time-independent quantity related to some average orientation of the NH-bond sampled over a very long time interval (milliseconds and longer). Relaxation rates, on the other hand, sense both the rates and magnitudes of fluctuations of the spin Hamiltonian, reflected in the corresponding correlation functions.

There has been significant interest recently in using RDC data for characterization of intraprotein dynamics.^{5,22–31} However, because RDCs can provide only time-independent information, all these analyses characterize not the protein dynamics *per se* but rather the distribution of bond orientations (caused by intraprotein motions) averaged over the time course of measurement. Even here, only relative, but not the absolute, amplitudes (or the corresponding order parameters) are available from RDC measurements; because of the tracelessness of the alignment tensor, the amplitudes are determined up to an arbitrary uniform scaling factor.

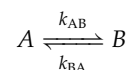
To summarize, the RDCs provide information about protein structure averaged over a very long time interval but cannot provide direct information about the timescale of motions involved, as this method samples equilibrium distribution of vector orientations. In contrast, spin-relaxation rates provide direct information about protein dynamics, because they directly probe time-dependent orientational correlation functions. However, the overall tumbling (usually in the several to tens of nanoseconds range) limits the longest correlation time of intraprotein motion detectable by this method. It should be mentioned that ¹⁵N relaxation rates also contain information on the equilibrium distribution of NH-bond orientations (although sampled in a narrower time range set by the overall tumbling rate), since this distribution determines the long-time limit of the relaxation-relevant correlation function.

Therefore, the main idea of the approach proposed here is to use spin-relaxation rates and RDCs simultaneously, as two complementary experimental data sets, in order to obtain, within the framework of a particular model, the information about protein domain reorientations on a timescale that extends beyond the cutoff set by the correlation time of protein's overall tumbling. In this case, RDC data can help refine the information about the equilibrium distribution of NH-bond orientations, and thus improve the description of ¹⁵N relaxation data.

THE MODEL OF MOTION

Motions of a dual-domain protein are described here within the framework of the ITS model.¹⁵ This model considers

three dynamic modes: overall diffusion, interdomain motion, and local, intradomain mobility, the latter being typically described as fast wobbling of a NH-bond. The main assumption of the model is that the two modes of intraprotein dynamics are statistically independent from each other and from the overall tumbling (see also Ref. 15). This model also assumes a particular process of interdomain mobility: a transition between two distinct conformational states of a protein (hereafter referred to as states *A* and *B*), with the rate constants k_{AB} and k_{BA} :



This type of protein dynamics affects ¹⁵N relaxation rates and RDCs in different ways.

The physical quantities typically measured in the relaxation experiments are the rates of longitudinal, R_1 , and transverse, R_2 , ¹⁵N relaxation which are related to cosine Fourier transform of the time-correlation function, $C(t)$.^{32,33} Within the framework of the ITS model $C(t)$ has the following form¹⁵ (also Ryabov and Fushman, in preparation):

$$\begin{aligned} C(t) &= \left\langle D_{q,0}^{(2)*}(\Omega_{L \rightarrow I}^0) D_{q,0}^{(2)}(\Omega_{L \rightarrow I}^t) \right\rangle_{L \rightarrow I} \\ &\cong \sum_{m=-2}^2 \sum_{n=-2}^2 \sum_{k=-2}^2 \sum_{l=-2}^2 \sum_{s=-2}^2 \sum_{h=-2}^2 \left\langle D_{q,m}^{(2)*}(\Omega_{L \rightarrow P}^0) D_{q,n}^{(2)}(\Omega_{L \rightarrow P}^t) \right\rangle_{L \rightarrow P} \\ &\quad \times \left\langle D_{m,k}^{(2)*}(\Omega_{P \rightarrow D}^0) D_{n,l}^{(2)}(\Omega_{P \rightarrow D}^t) \right\rangle_{P \rightarrow D} \\ &\quad \times D_{k,s}^{(2)*}(\Omega_{D \rightarrow R}) D_{l,h}^{(2)}(\Omega_{D \rightarrow R}) \left\langle D_{s,0}^{(2)*}(\Omega_{R \rightarrow I}^0) D_{h,0}^{(2)}(\Omega_{R \rightarrow I}^t) \right\rangle_{R \rightarrow I} \end{aligned} \quad (1)$$

where the three dynamic modes of ITS model are represented by the following correlation functions:

$$\text{overall tumbling: } \left\langle D_{q,m}^{(2)*}(\Omega_{L \rightarrow P}^0) D_{q,n}^{(2)}(\Omega_{L \rightarrow P}^t) \right\rangle_{L \rightarrow P} \quad (2a)$$

$$\text{interdomain motion: } \left\langle D_{m,k}^{(2)*}(\Omega_{P \rightarrow D}^0) D_{n,l}^{(2)}(\Omega_{P \rightarrow D}^t) \right\rangle_{P \rightarrow D} \quad (2b)$$

$$\text{local, intradomain mobility: } \left\langle D_{s,0}^{(2)*}(\Omega_{R \rightarrow I}^0) D_{h,0}^{(2)}(\Omega_{R \rightarrow I}^t) \right\rangle_{R \rightarrow I} \quad (2c)$$

In the above expressions $D_{m,n}^{(2)}(\Omega)$ is the element of Wigner rotation matrix, the angular brackets $\langle \dots \rangle$ mean an equilibrium ensemble averaging, Ω_s are different sets of Euler angles specifying a sequence of subsequent rotations (indicated by the subscripts) that result in a transition from the laboratory coordinate system (*L*) to the coordinate system associated with the instantaneous orientation of a NH-vector (*I*) (see Fig. 1), and superscripts '0' and 't' denote the initial and final time moments.

In the ITS model, the interdomain motion affects only the second step, $P \rightarrow D$; the corresponding term in $C(t)$, Eqn (2b), can be cast as:

$$\begin{aligned} &\left\langle D_{m,k}^{(2)*}(\Omega_{P \rightarrow D}^0) D_{n,l}^{(2)}(\Omega_{P \rightarrow D}^t) \right\rangle_{P \rightarrow D} \\ &= p_A \left(p(A|A, t) D_{m,k}^{(2)*}(\Omega_{P \rightarrow D}^A) D_{n,l}^{(2)}(\Omega_{P \rightarrow D}^A) \right) \end{aligned}$$

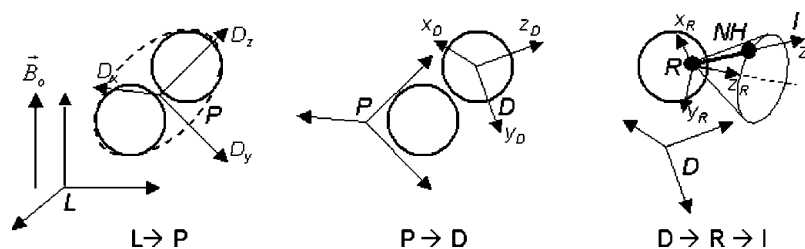


Figure 1. Schematic representation of a set of successive rotations that relate instant orientation of the NH-vector to the direction of the static magnetic field \vec{B}_0 (cf Eqn (1)): $L \rightarrow P$: from the laboratory frame L (aligned with \vec{B}_0) to the diffusion tensor frame P , characterized by the Euler angles $\Omega_{L \rightarrow P}$; $P \rightarrow D$: then to the coordinate frame D for each domain (e.g. PDB coordinate frame), characterized by the Euler angles $\Omega_{P \rightarrow D}$; $D \rightarrow R$: then to the residue-specific frame R , associated with the average orientation of the NH-vector, characterized by fixed Euler angles $\Omega_{D \rightarrow R}$ with respect to the domain's coordinate frame; and, finally, $R \rightarrow I$: to the instant frame I , attached to the NH-vector, the Euler angles are $\Omega_{R \rightarrow I}$. Although in the analysis presented in this paper the local backbone dynamics are ignored (Eqn (4) and hence we actually make no distinction between the R and I frames, we find it instructive to represent them here as separate frames, in order to preserve the generality of this picture.

$$\begin{aligned}
 & + p(A|B, t) D_{m,k}^{(2)*}(\Omega_{P \rightarrow D}^A) D_{n,l}^{(2)}(\Omega_{P \rightarrow D}^B) \\
 & + p_B \left(p(B|A, t) D_{m,k}^{(2)*}(\Omega_{P \rightarrow D}^B) D_{n,l}^{(2)}(\Omega_{P \rightarrow D}^A) \right. \\
 & \left. + p(B|B, t) D_{m,k}^{(2)*}(\Omega_{P \rightarrow D}^B) D_{n,l}^{(2)}(\Omega_{P \rightarrow D}^B) \right) \quad (3)
 \end{aligned}$$

Here $\Omega_{P \rightarrow D}^A$ and $\Omega_{P \rightarrow D}^B$ are the sets of Euler angles for states A and B ; $p_A = k_{BA}/(k_{AB} + k_{BA})$ and $p_B = k_{AB}/(k_{AB} + k_{BA})$ are the corresponding equilibrium occupation probabilities; $p(A|A, t) = p_A + p_B e^{-t/\tau_{ITS}}$ and $p(B|B, t) = p_B + p_A e^{-t/\tau_{ITS}}$ are the conditional probabilities to find the system at time t in the same state (A or B) as at $t = 0$; and $p(A|B, t) = p_B(1 - e^{-t/\tau_{ITS}})$ and $p(B|A, t) = p_A(1 - e^{-t/\tau_{ITS}})$ are the conditional probabilities to find the system in a different state (B or A) at time t . In these equations we introduced characteristic time of interconversion τ_{ITS} which is the reciprocal of the rate, $K = k_{AB} + k_{BA}$, of interconversion between the two states. Note a simple relationship between the rate constants and τ_{ITS} : $k_{AB} = (1 - p_A)/\tau_{ITS}$; $k_{BA} = p_A/\tau_{ITS}$.

The correlation functions describing overall rotational diffusion (Eqn (2a), $L \rightarrow P$) can be found in the original paper by Favro,³⁴ the famous Woessner's application³⁵ of Favro's results to protein tumbling, or in later reviews.^{36,37} Here we describe the overall tumbling using the correlation function for rotational diffusion of an anisotropic rigid body:³⁴

$$\left\langle D_{q,m}^{(2)*}(\Omega_{L \rightarrow P}^0) D_{q,n}^{(2)}(\Omega_{L \rightarrow P}^t) \right\rangle_{L \rightarrow P} = \frac{1}{5} \sum_{r=-2}^2 e^{-E_r t} a_{r,m}^* a_{r,n} \quad (4)$$

where $a_{r,m}$ are decomposition coefficients and E_r are the corresponding rate constants for the exponentials, both depend only on the principal values $\{D_x, D_y, D_z\}$ of the rotational diffusion tensor \underline{D} (see the Appendix). The properties of protein's tumbling are completely determined by its rotational diffusion tensor. For example, the overall correlation time of the protein is $\tau_c = [2(D_x + D_y + D_z)]^{-1}$.

The angles $\Omega_{D \rightarrow R}$ specifying the average orientation of the NH-vector with respect to the coordinate frame of the corresponding domain are assumed to be time-independent. Local dynamics of the NH-bond (Eqn (2c), $R \rightarrow I$) can be described using, e.g., the 'model-free' approach^{38,39} or can be ignored by setting:

$$\left\langle D_{s,0}^{(2)*}(\Omega_{R \rightarrow I}^0) D_{h,0}^{(2)}(\Omega_{R \rightarrow I}^t) \right\rangle_{R \rightarrow I} = \delta_{s,0} \delta_{h,0} \quad (5)$$

where $\delta_{i,j}$ is the Kronecker's delta. The latter approximation is justified here because in our analysis below we use the ratio of modified relaxation rates (Eqn (10)) which is insensitive, to a first approximation, to the local backbone dynamics mode.⁴ Thus in the current treatment, the local backbone dynamics are ignored, and therefore in the analysis below we make no distinction between the R and I frames for each amide.

Substituting Eqns (3–5) into Eqn (1) and taking analytical Fourier transform of the resulting correlation function, we obtain the following expression for the spectral density of the ITS model used in this study:

$$\begin{aligned}
 J(\omega) &= \frac{2}{5} \sum_{m=-2}^2 \sum_{n=-2}^2 \sum_{k=-2}^2 \sum_{l=-2}^2 \sum_{r=-2}^2 a_{r,m}^* a_{r,n} \\
 &\times \left\{ \frac{E_r}{E_r^2 + \omega^2} \left[p_B^2 D_{m,k}^{(2)*}(\Omega_{P \rightarrow D}^B) D_{n,l}^{(2)}(\Omega_{P \rightarrow D}^B) + p_A^2 D_{m,k}^{(2)*}(\Omega_{P \rightarrow D}^A) \right. \right. \\
 &\times D_{n,l}^{(2)}(\Omega_{P \rightarrow D}^A) + p_B p_A D_{m,k}^{(2)*}(\Omega_{P \rightarrow D}^B) D_{n,l}^{(2)}(\Omega_{P \rightarrow D}^A) \\
 &+ p_B p_A D_{m,k}^{(2)*}(\Omega_{P \rightarrow D}^A) D_{n,l}^{(2)}(\Omega_{P \rightarrow D}^B) \left. \right] + \frac{\tau_{ITS}(E_r \tau_{ITS} + 1) p_B p_A}{(E_r \tau_{ITS} + 1)^2 + (\omega \tau_{ITS})^2} \\
 &\times \left[D_{m,k}^{(2)*}(\Omega_{P \rightarrow D}^B) D_{n,l}^{(2)}(\Omega_{P \rightarrow D}^B) + D_{m,k}^{(2)*}(\Omega_{P \rightarrow D}^A) D_{n,l}^{(2)}(\Omega_{P \rightarrow D}^A) \right. \\
 &\left. - D_{m,k}^{(2)*}(\Omega_{P \rightarrow D}^B) D_{n,l}^{(2)}(\Omega_{P \rightarrow D}^A) - D_{m,k}^{(2)*}(\Omega_{P \rightarrow D}^A) D_{n,l}^{(2)}(\Omega_{P \rightarrow D}^B) \right] \left. \right\} \\
 &\times D_{k,0}^{(2)*}(\Omega_{D \rightarrow R}) D_{l,0}^{(2)}(\Omega_{D \rightarrow R}) \quad (6)
 \end{aligned}$$

A detailed description of the model will be published elsewhere (Ryabov and Fushman, in preparation).

In contrast to ^{15}N relaxation, a standard RDC experiment provides for a given pair of bonded nuclei, ^{15}N and ^1H , a value of the time-independent dipolar coupling, d ,

$$d = d_{\max}^{\text{NH}} \times (P_2(\cos \theta)) \quad (7)$$

where $P_2(\cos \theta) = \frac{1}{2}(3 \cos^2 \theta - 1)$ is the second-order Legendre polynomial, $d_{\max}^{\text{NH}} = 21.7$ kHz is the theoretical maximum for $^{15}\text{N}-^1\text{H}$ dipolar coupling (assuming NH-bond length of 1.04 Å), and the angle θ specifies the orientation of a NH-bond with respect to the direction of the static magnetic field \vec{B}_0 (laboratory reference frame L).^{5,19,40}

It is more convenient, however, to represent the averaged values of the Legendre polynomial from Eqn (7) through the

orientations of protein's NH-vectors with respect to some global reference frame (P) associated with the whole protein (we chose the principal axes frame of the overall diffusion tensor as the protein reference frame, P):

$$d = d_{\max}^{\text{NH}} \sum_{i,j=x,y,z} S_{ij} \cos \varphi_i \cos \varphi_j \quad (8)$$

where angles φ_i specify averaged orientations of a NH-bond (coordinate frame R), with respect to the corresponding axes of the molecular frame P and S_{ij} are components of the Saupe order matrix,⁴¹ $S_{ij} = \frac{3}{2}(\cos \Psi_i \times \cos \Psi_j) - \frac{1}{2}\delta_{ij}$. The angles Ψ_i here specify instantaneous orientation of the molecular frame P with respect to the director, assumed to coincide with the direction of the static magnetic field. In this representation, Eqn (8), all statistical orientational averaging usually occurs in the Saupe order matrix. In an isotropic medium, the overall tumbling of the protein makes all components of this matrix equal zero. A slight distortion of this symmetry introduced by protein's alignment results in nonzero components of the Saupe matrix. This matrix is traceless, $S_{xx} + S_{yy} + S_{zz} = 0$, and symmetric, $S_{ij} = S_{ji}$, which means that it can be completely determined by only five values: for instance its two eigenvalues S_{xx} and S_{yy} and three Euler angles, $\Omega_{P \rightarrow S}$, that specify orientations of the eigenvectors of the Saupe matrix (reference frame S) with respect to the protein's reference frame P . A so-called *alignment tensor* \underline{A} ^{5,40} is often used instead of the Saupe matrix in RDC data analysis. The two quantities are linearly related: $A_{ii} = (2/3)S_{ii}$; therefore, we will use them interchangeably where it does not cause any confusion.

By virtue of Eqns (7) and (8), RDC measurements probe time-independent equilibrium distribution of probability density function for orientations of NH vectors. Therefore, with respect to RDC measurements, all intraprotein dynamics (local, interdomain, etc.) can be regarded as infinitely fast processes. For the ITS model this means that the dipolar coupling measured for a given NH-bond can be considered as a simple population average between the two conformational states (A and B):

$$d = d_{\max}^{\text{NH}} \sum_{i,j=x,y,z} S_{ij} (p_A \cos \varphi_i^A \cos \varphi_j^A + p_B \cos \varphi_i^B \cos \varphi_j^B) \quad (9)$$

where angles φ_i^A and φ_i^B specify orientations of the NH-bond (frame R) in the conformational states A and B with respect to the overall molecular reference frame P . Within the framework of the ITS model the transition from reference frame P to reference frame R is given by two subsequent rotations $P \rightarrow D$ and $D \rightarrow R$. Thus, the direction cosines $\cos \varphi_i^A$ and $\cos \varphi_i^B$ can be derived directly from the Euler angles $\Omega_{P \rightarrow D}^A$ and $\Omega_{P \rightarrow D}^B$ which determine the orientations of a protein domain (in states A and B) with respect to the reference frame P , and (time-independent) angles $\Omega_{D \rightarrow R}$ that specify the time-averaged orientation of the NH-bond within the corresponding domain.

It is worth mentioning here that we assume that the system is already at equilibrium on the relaxation-relevant timescale (nanoseconds), i.e. no additional motions occur that could influence the RDCs but not the ¹⁵N relaxation

data. Note that Eqn (9) also assumes that the interdomain dynamics is fast on the timescale relevant for establishing the Saupe order matrix of the protein (*cf* Eqn (8)), such that both conformations of Ub₂ have the same alignment tensor.

Because both ¹⁵N relaxation data and RDCs depend on parameters of the same ITS model (see Eqns (1), (3), (6) and (9)), these data sets can be used for simultaneous characterization of the orientation and dynamics of protein domains. It should be emphasized in this regard that such a treatment is possible only when the alignment does not affect the protein's structure (conformation) and interdomain dynamics, i.e. the protein's behavior is identical during the RDC and NMR relaxation experiments. Although this is a typical assumption made in all RDC data analyses,^{5,14,19,22–30} it is difficult to prove it rigorously since little is known about the alignment process itself. In the case of Ub₂, this assumption is supported by the good agreement between static interdomain orientations derived from RDC and relaxation data, analyzed for each Ub domain separately.^{8,16} Therefore, we will assume that the aligning medium does not introduce significant changes in the protein's structure and dynamics.

MATERIALS AND METHODS

Both ¹⁵N relaxation and RDC data were collected for Lys48-linked Ub₂ at pH 6.8, 24 °C and 14.1 Tesla, as reported earlier.^{8,16} Throughout this paper, the Ub unit that carries the free C-terminus is referred to as the 'proximal' domain, while the other Ub unit in Ub₂ is called 'distal'. Thus, the two Ub molecules in Ub₂ are linked via an isopeptide bond between the C-terminal Gly76 of the distal Ub and Lys48 of the proximal Ub. Ub₂ chains ¹⁵N-labeled at the proximal or distal domain were assembled from recombinant Ub molecules (unlabeled and ¹⁵N-labeled) using segmental isotope labeling strategy detailed elsewhere.¹⁶

The NMR relaxation data used in this study comprise ¹⁵N relaxation rates ($R_1 = 1/T_1$ and $R_2 = 1/T_2$) and steady-state heteronuclear {¹H} ¹⁵N NOEs. As aligning medium for RDC experiments we used a mixture of *n*-alkyl-poly(ethylene glycol) (C₁₂E₅) and *n*-hexanol (molar ratio 0.85) added to the buffer solution at 5 wt%.⁴²

For the analyses of these experimental data we used the solution NMR structure of monomeric ubiquitin (PDB entry 1D3Z, model 1) as the structure model for each domain in Ub₂. The original 1D3Z coordinates were rotated by Euler angles {90°, 90°, 180°} to avoid having $\beta_{P \rightarrow D} \sim 0$ or 180° when the angles $\alpha_{P \rightarrow D}$ and $\gamma_{P \rightarrow D}$ cannot be accurately separated (see details elsewhere¹⁵).

In total, 70 amides were included in the analysis of ¹⁵N relaxation data; they belong to residues 2–6, 12–17, 21, 28, 32–34, 36, 39–45, 49, 50, 57–59, 61, 64–67 and 69 in the proximal domain and 2–4, 13–18, 26–30, 32–36, 40–43, 45, 48–50, 54, 57, 59 and 65–69 in the distal Ub. The 69 residues included in the RDC data analysis were 2–6, 12–17, 25, 26, 28–34, 39–42, 45, 57–59, 66, 67, 70 and 71 (proximal Ub) and 2–6, 13–17, 23, 25–34, 39–45, 57–59 and 66–71 (distal Ub).

The analysis of ^{15}N relaxation data was performed by fitting the ratio of experimentally measured parameters

$$\rho = \frac{R'_1}{2R'_2 - R'_1} \quad (10)$$

to its theoretical value calculated from the expression $\rho = (3/4)J(\omega_N)/J(0)$. Here R'_1 and R'_2 are the modified rates of longitudinal and transverse ^{15}N relaxation, respectively:⁸ $R'_1 = R_1[1 - 1.249|\gamma_N/\gamma_H|(1 - \text{NOE})]$; $R'_2 = R_2 - 1.079|\gamma_N/\gamma_H|R_1(1 - \text{NOE})$; $J(\omega)$ is the spectral density, γ_N and γ_H are gyromagnetic ratios of nitrogen and hydrogen nuclei, and ω_N is the ^{15}N Larmor frequency. This modification corresponds to subtraction of the contributions to relaxation rates from the high-frequency components of the spectral density. The quantity ρ is independent of the site-specific variations in the ^{15}N chemical shift anisotropy and, for protein core elements, of the order parameters of local backbone motion.⁸

Both ^{15}N relaxation and RDC data were analyzed within the framework of the ITS model using in-house software. The goodness of the fits was characterized by the χ^2 values for relaxation (χ^2_{relax}) and RDC (χ^2_{RDC}) data, normalized by the corresponding number of degrees of freedom (DoF_{relax} and DoF_{RDC}):

$$\chi^2_{\text{relax}} = \frac{1}{DoF_{\text{relax}}} \sum_f \left(\frac{\rho_f^{\text{exp}} - \rho_f^{\text{calc}}}{\sigma_f^{\text{relax}}} \right)^2 \quad (11a)$$

$$\chi^2_{\text{RDC}} = \frac{1}{DoF_{\text{RDC}}} \sum_g \left(\frac{d_g^{\text{exp}} - d_g^{\text{calc}}}{\sigma_g^{\text{RDC}}} \right)^2 \quad (11b)$$

where indices f and g enumerate residues included in the analysis of relaxation and RDC data, respectively; superscripts 'exp' and 'calc' denote experimentally measured and back-calculated values; σ_f^{relax} are residue-specific absolute experimental errors in ρ ; the experimental errors in the RDC data, σ_g^{RDC} , were assumed to be uniform and equal to 3 Hz. The data analysis includes 17 fitting parameters for ITS model and five fitting parameters that describe the alignment tensor, thus, $DoF_{\text{relax}} = 53$ and $DoF_{\text{RDC}} = 64$. We employed different fitting strategies, using χ^2_{relax} and χ^2_{RDC} separately and in combination, as described in the next section.

Confidence intervals for fitted parameters were estimated using χ^2 boundary (for the alignment tensor in Table 1a) and bootstrap (all other parameters in Table 1a and all parameters in Table 1b) methods.⁴³ The latter method, becoming increasingly popular for confidence interval estimations in complex systems, is based on the idea of using the original experimental data set to generate a number of synthetic data sets in which a certain fraction of the original data points ($1/e \approx 37\%$) is replaced by randomly chosen duplicates of the remaining data. Thus, these synthetic data sets should have the same statistical properties as the original

Table 1a. Parameters of the ITS model and the alignment tensor of Ub₂ in the case when interdomain dynamics were analyzed using ^{15}N relaxation data only

| Parameters of the ITS model ($\chi^2_{\text{relax}} = 1.69$) | | | | | | | | | | | | |
|---|---------|---------|--|---------|----------|---|--|---|---|--|---|------------------------------|
| D_x^a | D_y^a | D_z^a | τ_{ITS}^b | p_A^c | Domain | $\alpha_{P \rightarrow D}^A$ ^d | $\beta_{P \rightarrow D}^A$ ^d | $\gamma_{P \rightarrow D}^A$ ^d | $\alpha_{P \rightarrow D}^B$ ^d | $\beta_{P \rightarrow D}^B$ ^d | $\gamma_{P \rightarrow D}^B$ ^d | |
| 1.53 | 1.73 | 2.20 | 9.3 | 0.90 | Proximal | 218 (35) | 109 (11) | 140 (4) | 203 (38) | 110 (9) | 72 (8) | |
| (0.32) | (0.06) | (0.08) | (4.8) | (0.06) | Distal | 91 (28) | 58 (7) | 321 (19) | 156 (33) | 96 (38) | 356 (33) | |
| Parameters of the alignment tensor ($\chi^2_{\text{RDC}} = 3.22$) | | | | | | | | | | | | |
| $d_{\text{max}}^{\text{NH}} \times S_{xx}^e$ | | | $d_{\text{max}}^{\text{NH}} \times S_{yy}^e$ | | | $\alpha_{P \rightarrow S}^f$ | | | $\beta_{P \rightarrow S}^f$ | | | $\gamma_{P \rightarrow S}^f$ |
| 8.8 (0.5) | | | 11.9 (0.4) | | | -23 (9) | | | 78 (1) | | | 19 (1) |

Table 1b. Parameters of the ITS model and the alignment tensor of Ub₂ in the case when interdomain dynamics were analyzed using ^{15}N relaxation and RDC data simultaneously

| Parameters of the ITS model ($\chi^2_{\text{relax}} = 1.77$) | | | | | | | | | | | | |
|---|---------|---------|--|---------|----------|---|--|---|---|--|---|------------------------------|
| D_x^a | D_y^a | D_z^a | τ_{ITS}^b | p_A^c | Domain | $\alpha_{P \rightarrow D}^A$ ^d | $\beta_{P \rightarrow D}^A$ ^d | $\gamma_{P \rightarrow D}^A$ ^d | $\alpha_{P \rightarrow D}^B$ ^d | $\beta_{P \rightarrow D}^B$ ^d | $\gamma_{P \rightarrow D}^B$ ^d | |
| 1.57 | 1.75 | 2.39 | 36.0 | 0.76 | Proximal | 287 (22) | 131 (8) | 153 (7) | 258 (28) | 115 (10) | 88 (12) | |
| (0.12) | (0.06) | (0.08) | (9.8) | (0.07) | Distal | 72 (15) | 52 (8) | 327 (8) | 147 (21) | 87 (21) | 356 (16) | |
| Parameters of the alignment tensor ($\chi^2_{\text{RDC}} = 0.49$) | | | | | | | | | | | | |
| $d_{\text{max}}^{\text{NH}} \times S_{xx}^e$ | | | $d_{\text{max}}^{\text{NH}} \times S_{yy}^e$ | | | $\alpha_{P \rightarrow S}^f$ | | | $\beta_{P \rightarrow S}^f$ | | | $\gamma_{P \rightarrow S}^f$ |
| 7.3 (1.3) | | | 18.5 (3.2) | | | -52 (23) | | | 95 (8) | | | 11 (6) |

Numbers in the parentheses represent estimated uncertainties in the parameters.

^a Principal components, D_x , D_y , and D_z , of the overall rotational diffusion tensor, in 10^7 s^{-1} (ordered as $D_x \leq D_y \leq D_z$).

^b Characteristic time constant for the interconversion between the two states, $\tau_{\text{ITS}} = 1/K$, in ns.

^c Occupation probability for the more populated state (here called state A); the occupation probability for state B is $p_B = 1 - p_A$.

^d The Euler angles, in degrees, specifying for the states A and B the orientation of the PDB frame for each Ub domain with respect to the principal axes frame of the overall rotational diffusion tensor.

^e Eigenvalues of the Saupe matrix multiplied by the maximal strength of the ^{15}N - ^1H dipolar coupling, in Hz. The third eigenvalue can be obtained from the zero-trace condition, $S_{xx} + S_{yy} + S_{zz} = 0$.

^f The Euler angles, in degrees, specifying the orientation of the principal axes frame of the Saupe order matrix with respect to the reference frame of the overall rotational diffusion tensor.

one. At least 200 sets of synthetic data were generated in each case. These synthetic data were analyzed in the same way as the original data, and the confidence intervals reported here were obtained from the resulting distributions of the values of fitting parameters.

RESULTS AND DISCUSSION

In our previous study¹⁵ (also Ryabov and Fushman, in preparation) we extensively explored the situation when interdomain dynamics of Ub₂ were analyzed from ¹⁵N relaxation data only, using a fitting procedure that minimizes χ_{relax}^2 . The parameters of ITS model obtained from this analysis are presented in Table 1a. In contrast, a single set of RDC data measured for one aligning medium cannot be used alone to obtain parameters of the ITS model. The principal reason for this, as already mentioned above, is the absence of dynamic information in RDC data. In addition, owing to the tracelessness of the alignment tensor, it is impossible to resolve the individual contributions from the conformations *A* and *B* to their linear combination in Eqn (9). However, RDC data can be used to validate the results obtained from NMR relaxation data. This can be done by substituting into Eqn (9) the occupation probabilities and the direction cosines obtained from relaxation data analysis. Then, the components of alignment tensor can be obtained using the singular value decomposition method,⁴⁴ which provides the best possible agreement (minimal χ_{RDC}^2) between experimental and back-calculated RDC values for

these particular structures and their occupation probabilities. The parameters of the alignment tensor derived in such a way are also presented in Table 1a.

As one can see from Fig. 2(a) this treatment results in a good agreement between experimental and back-calculated relaxation data with a reasonably high Pearson's correlation coefficient ($r = 0.95$). However, the agreement between experimental and back-calculated RDCs in this case is drastically worse (Fig. 2(b)), which indicates that the structures and occupation probabilities derived from the relaxation data alone do not fit well the RDC data.

In order to explore the reasons for this disagreement, we analyzed the RDC and relaxation data simultaneously. In this case, at each iteration step of the fitting procedure the current values of Euler angles, $\Omega_{P \rightarrow D}^A$ and $\Omega_{P \rightarrow D}^B$, and occupation probabilities, p_A and p_B , were used both for calculating the ¹⁵N relaxation data and for determining the alignment tensor. This fitting minimized the sum, $\chi_{\text{relax}}^2 + \chi_{\text{RDC}}^2$. The corresponding values of all adjustable parameters of the ITS model and the alignment tensor are presented in Table 1b. This treatment resulted in a remarkable improvement in the agreement between the experimental and back-calculated RDCs, as shown in Fig. 2(d), with the correlation coefficient of 0.94 and the quality factor $Q = 0.23$ (down from 0.58 in Fig. 2(b)). The simultaneous analysis of ¹⁵N relaxation and RDC data also led to significant, more than sixfold, reduction in χ_{RDC}^2 . It is worth mentioning that this significant improvement in the RDC fit was reached at the cost of only a slight deterioration of the relaxation data fit: χ_{relax}^2 increased

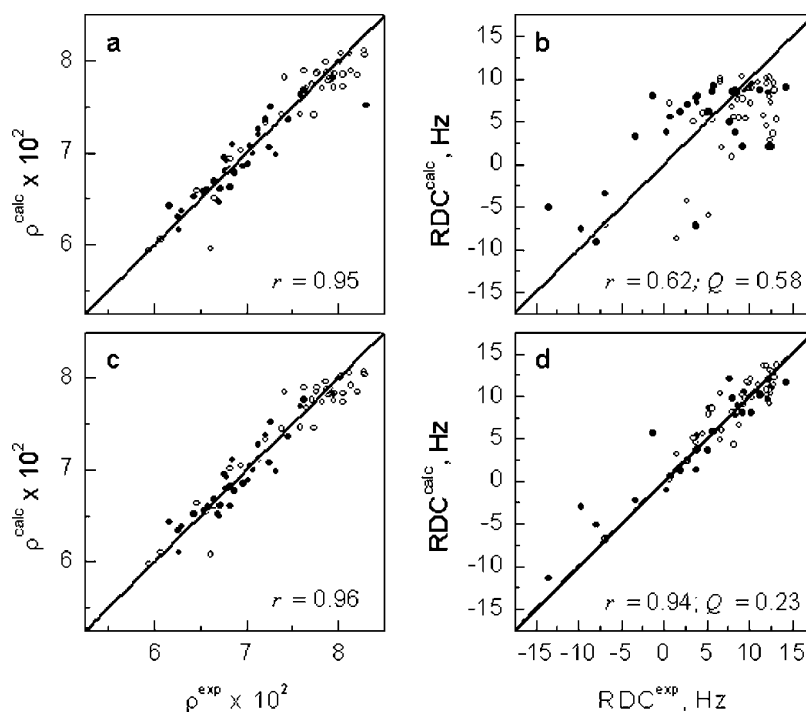


Figure 2. The agreement between experimental ('exp') and back-calculated ('calc') values of (a), (c) ¹⁵N relaxation data (presented in terms of the ratio ρ of relaxation rates, Eqn (10)) and (b), (d) residual dipolar couplings. The upper panels, (a) and (b), correspond to the ITS analysis of ¹⁵N relaxation data alone. Here, the structures derived from this fit were used as input for treating the RDC data. Lower panels, (c) and (d), represent the results of the simultaneous analysis of the relaxation and RDC data. In all the panels, solid symbols are for the proximal domain, open symbols are for distal domain, and solid lines are guides-for-the-eye representing the case of absolute correlation. r is the Pearson's correlation coefficient; Q is the quality factor⁴⁵ for RDC data.

by less than 5% (Table 1), while the correlation between the experimental and back-calculated relaxation data remained at the same high level.

To rationalize this finding let us take a closer look at the dynamic parameters of the ITS model presented in Table 1. Specifically, the overall rotational correlation time and the interconversion time derived from ^{15}N relaxation data alone are very close to each other: $\tau_c = 9.2$ ns and $\tau_{ITS} = 9.3$ ns (Table 1a). In contrast, when the relaxation and RDC data were analyzed together, the time of interconversion became 4-fold longer than the overall correlation time: $\tau_c = 8.8$ ns and $\tau_{ITS} = 36.0$ ns (Table 1b). These results are consistent with the idea that the relaxation rates are not sensitive to reorientational motion that is much slower than the overall tumbling; hence the interconversion time derived from spin-relaxation data alone cannot be considerably longer than τ_c . The inclusion of the RDCs that sense the cumulative effect of reorientations occurring on a much longer timescale thus allowed us to refine the parameters of the ITS model (see also below) such that it nicely fits both sets of data, at the cost of τ_{ITS} getting somewhat longer than the overall correlation time. These findings illustrate the idea that simultaneous analysis of NMR relaxation and RDC data can provide information about interdomain mobility in the case when $\tau_{ITS} \geq \tau_c$.

Note that this approach might be in trouble when significant motions (e.g. slow loop dynamics or other intra domain motions) not related to interdomain reorientation occur on a timescale slower than the overall tumbling (hence reflected in RDCs but not in relaxation data), because treating the data using a model that does not take these motions into account could result in erroneous estimates for the ITS parameters. As shown in Ref. 16, the interdomain orientations obtained by aligning the individual Ub domains in Ub₂ on the basis of separate (static) analyses of the RDCs and the ^{15}N relaxation data are very similar. This indicates that the presence of such intradomain motions in Ub₂ that would noticeably affect the RDCs but not the relaxation data is unlikely.

It can be argued that the value of interconversion time derived from simultaneous analysis of RDC and relaxation data is too slow to be accurately determined from the fitting procedure. If this was the case, then replacing the actual correlation function of interdomain motion, Eqn (3), with a simple population averaging between conformations *A* and *B* should fit the experimental data equally well. This would be the case when the interconversion is much slower than the overall tumbling, yet fast enough on the spin-relaxation timescale, such that the apparent spin-relaxation rate is a simple population average of the corresponding rates in the two conformations. In this case the dynamic nature of the process of interconversion can be neglected, which can be achieved within the ITS model either by neglecting the $e^{-t/\tau_{ITS}}$ terms in the conditional probabilities in Eqn (3) or by setting $\tau_{ITS} \rightarrow \infty$ in the final expression for the spectral density, Eqn (6). Thus, to further validate the obtained value for the interconversion time ($\tau_{ITS} = 36.0$ ns) we performed a control fit in which τ_{ITS} was held constant, at a value much longer than the tumbling time: $\tau_{ITS} = 1$ s. This resulted in a significant increase in the normalized χ^2 values (about 36% for χ_{relax}^2 and about 49% for χ_{RDC}^2), which

indicates a substantial worsening of the fit. In addition, the obtained eigenvalues of the overall diffusion tensor, $D_x = 0.99 \times 10^7 \text{ s}^{-1}$, $D_y = 2.32 \times 10^7 \text{ s}^{-1}$ and $D_z = 3.10 \times 10^7 \text{ s}^{-1}$, correspond to an oblate tumbling object, which contradicts the prolate shape of the Ub₂ molecule. Similar numbers were obtained when setting τ_{ITS} to 1 μs . These results clearly validate the derived value of the interconversion time.

The structures of Ub₂ in the two conformations derived from the data presented in Table 1a and 1b are depicted in Fig. 3. Here both sets of conformations, Fig. 3(a), (b) and (c), (d), represent a transition between a conformation of Ub₂, where functionally important hydrophobic residues Leu8-Ile44-Val70 are sequestered at the interdomain interface (henceforth referred to as the 'closed' conformation), and an 'open' conformation, where these residues are exposed for possible interactions with various ligands. It should be mentioned that the methods used here provide only the relative orientation of the two domains, not their position with respect to each other, as no constraints are imposed on the translational degrees of freedom of the two domains. The domains in Fig. 3 are positioned somewhat arbitrarily with respect to each other, such that the flexible C-terminus of the distal Ub is close to Lys48 of the proximal Ub. However, the orientations of Ub domains in the closed conformations depicted in Fig. 3(a) and (c), where the hydrophobic patches (Leu8-Ile44-Val70) on both domains face each other, agree well with chemical shift perturbation data¹⁶ that indicate a well-defined Ub-Ub interface formed by the hydrophobic patches on both Ub domains in Ub₂ at pH 6.8. Also the derived values of the occupation probability of the closed state, $p_A = 0.90 \pm 0.06$ (Table 1a) and 0.76 ± 0.07 (Table 1b), are in fair agreement with the population number of 85% for the closed conformation¹⁶ estimated from the changes in chemical shift perturbations in Ub₂ (vs monomeric Ub) observed upon pH titration. Note also that the interdomain orientation in the 'closed' state generally agrees with the crystal structure of Ub₂,⁴⁶ which likely represents a snapshot of Ub₂ in the closed conformation.

The differences in the domain orientations between states *A* and *B* can be visualized as a rotation of each domain about a certain axis, as shown in Fig. 3. The rotation angles are 65° for the proximal Ub and 87° for the distal domain in the Ub₂ conformations derived solely from relaxation data. The corresponding rotation angles from simultaneous analysis of the relaxation and RDC data are 56° for the proximal and 85° for the distal Ub. There is also a difference between the two sets of Ub₂ conformations (Fig. 3) in the orientation of the rotation axes, mostly pronounced for the proximal Ub. Otherwise, the rotations associated with the *A* ↔ *B* interconversion are similar in the sense that in both domains the rotation axes go through the linkage region, i.e. the C-terminus of the distal Ub and Lys48 of the proximal Ub. This is consistent with the expected role of the Ub-Ub linker as a pivot point in the interdomain reorientations.

Which set of Ub₂ conformations is more accurate? As follows from the above discussion, the relaxation-only and the relaxation + RDC derived Ub₂ conformations both are in reasonable agreement with the existing experimental data. For example, as mentioned earlier, both structures in the

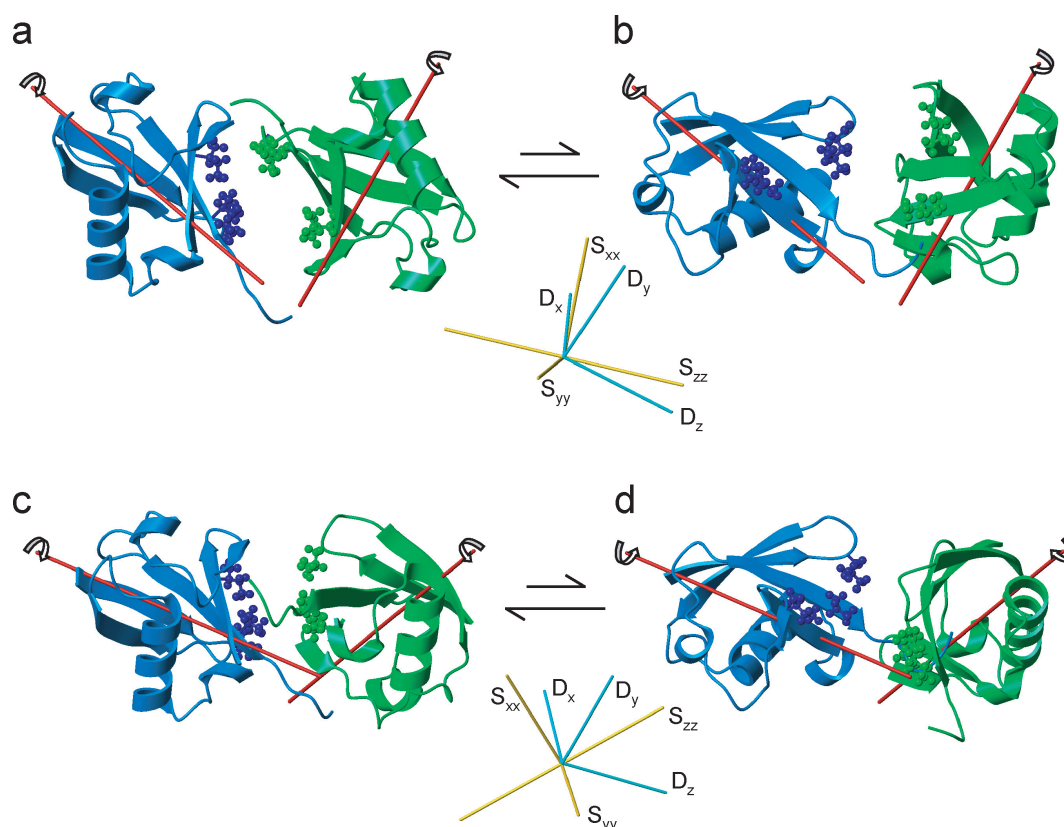


Figure 3. Cartoon representations of di-ubiquitin structures in the closed (a) and (c) and open (b) and (d) conformations. Structures in the panels (a) and (b) were obtained from ^{15}N relaxation data only (Table 1a), whereas those in panels (c) and (d) were derived from simultaneous analysis of the relaxation and RDC data (Table 1b). In all the panels, proximal domains are colored green, distal domains are blue; the hydrophobic residues Leu8, Ile44, and Val70 are shown in ball-and-stick. Cyan rods represent the orientation of the overall rotational diffusion tensor (reference frame P); gold rods show the principal axes of the Saupe order matrix (reference frame S). The red rods represent the axes of rotation for each domain and the curved arrows indicate the direction of rotation towards the other state. For the structures derived solely from relaxation data (panels (a) and (b)) the rotation angles are 65° and 87° for the proximal and distal domains, respectively. Simultaneous analysis of the relaxation and RDC data (c), (d) yielded the rotation angles of 56° (proximal Ub) and 85° (distal Ub).

closed conformation agree with the location of the observed chemical shift perturbations¹⁶ and bear general resemblance to the crystal structure⁴⁶ of Ub₂. While neither of the interdomain orientations in Fig. 3(a) and (c) overlays exactly with the crystal structure, the Ub₂ conformation from relaxation-only data is in a somewhat better agreement. On the other hand, the 'open' conformation (Fig. 3(d)) derived from simultaneous analysis of RDC and relaxation data is in good agreement with the Ub₂ conformation in the Ub₂/UBA complex: the two Ub₂ structures superimpose with the backbone rmsd of 1.7 Å (after superimposing centers of mass of the corresponding domains). In addition, both 'closed' conformations are in agreement with the pattern of signal attenuations observed in the proximal domain when a paramagnetic spin label was attached to Cys48 in the distal domain.¹⁵ The existing data are insufficient to decide in favor of a particular set of Ub₂ conformations, and additional information is required in order to address this issue. However, on the basis of the results discussed in this paper we would regard the structures derived from the simultaneous analysis of ^{15}N relaxation and RDC data (Fig. 3(c) and (d)) as more refined structures since they satisfy both experimental data sets. In terms of interdomain orientation, this was achieved by a tilt in the orientation

of the proximal domain and its rotation axis as can be seen from Fig. 3 and Table 1. In addition, a comparison of Table 1a and 1b indicates that the estimated uncertainties in the ITS parameters are generally slightly smaller when the RDC data are included in the analysis. Although not a dramatic improvement in the confidence intervals, this still suggests that simultaneous analysis of the relaxation and RDC data provided a more refined picture of the mechanism of domain reorientation in Ub₂.

CONCLUSIONS

Here, we demonstrated that NMR relaxation data and RDCs could be used as two complementary experimental data sets for characterization of interdomain mobility in a multidomain protein. The analysis of experimental data for Lys48-linked Ub₂ presented here shows that in the case when $\tau_{ITS} \geq \tau_c$, simultaneous analysis of spin relaxation and RDC data provides information about interdomain mobility, which could not be derived from separate analysis of either data set. Concluding this paper, we would also like to mention some possible future directions. First, one should note that the data treatment described above neglects fast

local dynamics of NH-bonds, because it is focused on the analysis of the ratio ρ of relaxation rates. It is obvious, however, that the information about order parameters of fast local motion is present both in the RDC data and in the ^{15}N relaxation rates. Therefore, including this dynamic mode into the analysis might provide additional useful information about intradomain motions. Secondly, as has already been mentioned, it is impossible to characterize even mutual domain orientation in both states of the ITS model using a single set of RDC data measured in a single aligning medium. Simultaneous analysis of several sets of RDC data collected in different aligning media can be useful in this regard. For example, recently developed methods of analysis of the amplitudes of local motions from RDC data measured in sufficient number of different aligning media (see e.g. Refs 23,30,31) can be extended to the analysis of domain motions. However, even in this case from RDC data alone, one can characterize only mutual orientations of protein domains in different conformational states but not the actual dynamics, i.e. the corresponding correlation times. Finally, the simple ITS model considered here will have to be extended to allow for more than two conformational states, in order to more accurately describe the 'open' conformations of Ub₂ and other multidomain systems.

Acknowledgements

This work was supported by NIH grant GM65334 to DF. The atom coordinates for the Ub₂ conformations are available from the authors upon request, and will be deposited with the Protein Data Bank.

APPENDIX

The values of the rate constants E_r in Eqn (4) are given by the following expressions:

$E_0 = 6D_s - 2\Delta$, $E_1 = 3(D_x + D_s)$, $E_{-1} = 3(D_y + D_s)$, $E_2 = 6D_s + 2\Delta$, $E_{-2} = 3(D_z + D_s)$, where $D_s = (D_y + D_x + D_z)/3$ and $\Delta = \sqrt{(D_y - D_x)^2 + (D_z - D_x)(D_z - D_y)}$. The values of $a_{r,m}$ are given in the following Table A1, where $N = 2\sqrt{|\Delta w|}$, $u = \sqrt{3}(D_x - D_y)$, and $w = 2D_z - D_x - D_y + 2\Delta$. Although it is usually assumed that $D_z \geq D_y \geq D_x$, these equations hold for any relationship between the principal components of the diffusion tensor, except for a very specific case of an axially symmetric oblate tensor with $D_z < D_x = D_y$, for which the expressions for Δ and w should change their sign: $\Delta = -\sqrt{(D_y - D_x)^2 + (D_z - D_x)(D_z - D_y)}$ and $w = -2D_z + D_x + D_y - 2\Delta$.

Table A1. Values of the decomposition coefficients $a_{r,m}$ that appear in Eqn (4)

| | 2 | 1 | m 0 | -1 | -2 |
|-----|------------------------|----------------------|---------------|-----------------------|------------------------|
| r | $\frac{w}{N\sqrt{2}}$ | 0 | $\frac{u}{N}$ | 0 | $\frac{w}{N\sqrt{2}}$ |
| | 0 | $\frac{1}{\sqrt{2}}$ | 0 | $\frac{1}{\sqrt{2}}$ | 0 |
| | $-\frac{u}{N\sqrt{2}}$ | 0 | $\frac{w}{N}$ | 0 | $-\frac{u}{N\sqrt{2}}$ |
| | 0 | $\frac{1}{\sqrt{2}}$ | 0 | $-\frac{1}{\sqrt{2}}$ | 0 |
| | $\frac{1}{\sqrt{2}}$ | 0 | 0 | 0 | $-\frac{1}{\sqrt{2}}$ |

REFERENCES

- Sicheri F, Kuriyan J. *Curr. Opin. Struct. Biol.* 1997; **7**: 777.
- Pickford AR, Campbell ID. *Chem. Rev.* 2004; **104**: 3557.
- Zhang Y, Zuiderweg ER. *Proc. Natl. Acad. Sci. U.S.A.* 2004; **101**: 10272.
- Fushman D, Xu R, Cowburn D. *Biochemistry* 1999; **38**: 10225.
- Fischer MWF, Losonczi JA, Weaver LJ, Prestegard JH. *Biochemistry* 1999; **38**: 9013.
- Skrynnikov N, Goto N, Yang D, Choy W, Tolman J, Mueller G, Kay L. *J. Mol. Biol.* 2000; **295**: 1265.
- Goto NK, Skrynnikov NR, Dahlquist FW, Kay LE. *J. Mol. Biol.* 2001; **308**: 745.
- Fushman D, Varadan R, Assfalg M, Walker O. *Prog. NMR Spectrosc.* 2004; **44**: 189.
- Varadan R, Assfalg M, Raasi S, Pickart C, Fushman D. *Mol. Cell.* 2005; **18**: 687.
- Baber JL, Szabo A, Tjandra N. *J. Am. Chem. Soc.* 2001; **123**: 3953.
- Chang SL, Tjandra N. *J. Am. Chem. Soc.* 2001; **123**: 11484.
- Chang SL, Szabo A, Tjandra N. *J. Am. Chem. Soc.* 2003; **125**: 11379.
- Clore GM, Szabo A, Bax A, Kay LE, Driscoll PC, Gronenborn AM. *J. Am. Chem. Soc.* 1990; **112**: 4989.
- Bertini I, Del Bianco C, Gelis I, Katsaros N, Luchinat C, Parigi G, Peana M, Provenzani A, Zoroddu MA. *Proc. Natl. Acad. Sci. U.S.A.* 2004; **101**: 6841.
- Ryabov Y, Fushman D. *Proteins* 2006; DOI: 10.1002/prot.20917.
- Varadan R, Walker O, Pickart C, Fushman D. *J. Mol. Biol.* 2002; **324**: 637.
- Tolman JR, Flanagan JM, Kennedy MA, Prestegard JH. *Proc. Natl. Acad. Sci. U.S.A.* 1995; **92**: 9279.
- Kung HC, Wang KY, Goljer I, Bolton PH. *J. Magn. Reson., Ser. B* 1995; **109**: 323.
- Tjandra N, Bax A. *Science* 1997; **278**: 1111.
- Tycko R, Blanco FJ, Ishii Y. *J. Am. Chem. Soc.* 2000; **122**: 9340.
- Meier S, Haussinger D, Grzesiek S. *J. Biomol. NMR* 2002; **24**: 351.
- Tolman JR. *Curr. Opin. Struct. Biol.* 2001; **11**: 532.
- Meiler J, Prompers JJ, Peti W, Griesinger C, Bruschweiler R. *J. Am. Chem. Soc.* 2001; **123**: 6098.
- Peti W, Meiler J, Bruschweiler R, Griesinger C. *J. Am. Chem. Soc.* 2002; **124**: 5822.
- Tolman JR. *J. Am. Chem. Soc.* 2002; **124**: 12020.
- Hus JC, Peti W, Griesinger C, Bruschweiler R. *J. Am. Chem. Soc.* 2003; **125**: 5596.
- Meiler J, Peti W, Griesinger C. *J. Am. Chem. Soc.* 2003; **125**: 8072.
- Bernado P, Blackledge M. *J. Am. Chem. Soc.* 2004; **126**: 4907.
- Bernado P, Blackledge M. *J. Am. Chem. Soc.* 2004; **126**: 7760.
- Blackledge M. *Prog. NMR Spectrosc.* 2005; **46**: 23.
- Bouvignies G, Bernado P, Meier S, Cho K, Grzesiek S, Bruschweiler R, Blackledge M. *Proc. Natl. Acad. Sci. U.S.A.* 2005; **102**: 13885.
- Abragam A. *The Principles of Nuclear Magnetism*. Clarendon Press: Oxford, 1961.
- Woessner D. *J. Chem. Phys.* 1961; **36**: 1.
- Favro DL. *Phys. Rev.* 1960; **119**: 53.
- Woessner D. *J. Chem. Phys.* 1962; **37**: 647.
- Huntress WT Jr. *Adv. Magn. Reson.* 1970; **4**: 1.
- Korzhnev DM, Billeter M, Arseniev AS, Orekhov VY. *Prog. Nucl. Magn. Reson. Spectrosc.* 2001; **38**: 197.
- Lipari G, Szabo A. *J. Am. Chem. Soc.* 1982; **104**: 4546.
- Lipari G, Szabo A. *J. Am. Chem. Soc.* 1982; **104**: 4559.
- Bax A, Kontaxis G, Tjandra N. *Methods Enzymol.* 2001; **339**: 127.
- Saupe A. *Angew. Chem., Int. Ed. Engl.* 1968; **7**: 97.
- Ruckert M, Otting G. *J. Am. Chem. Soc.* 2000; **122**: 7793.
- Press WH, Teukolsky SA, Vetterling WT, Flannery BP. *Numerical Recipes in C*. Cambridge University Press: New York, 1992.
- Losonczi JA, Andrec M, Fischer MW, Prestegard JH. *J. Magn. Reson.* 1999; **138**: 334.
- Ottiger M, Bax A. *J. Biomol. NMR* 1999; **13**: 187.
- Cook WJ, Jeffrey LC, Carson M, Zhijian C, Pickart CM. *J. Biol. Chem.* 1992; **267**: 16467.